Modelling multiphase flow inside the porous media of a polymer electrolyte membrane fuel cell

T. Berning & S. K. Kær
Department of Energy Technology, Aalborg University, Denmark

Abstract

Transport processes inside polymer electrolyte membrane fuel cells (PEMFC's) are highly complex and involve convective and diffusive multiphase, multispecies flow through porous media along with heat and mass transfer and electrochemical reactions in conjunction with water transport through an electrolyte membrane. We will present a computational model of a PEMFC with focus on capillary transport of water through the porous layers and phase change and discuss the impact of the liquid phase boundary condition between the porous gas diffusion layer and the flow channels, where water droplets can emerge and be entrained into the gas stream.
Keywords: fuel cell modelling, multi-phase flow, GDL/channel interface.

1 Introduction

Polymer electrolyte membrane fuel cells (PEMFC's) combine hydrogen with oxygen from air in order to generate electricity with the only by-products being water and waste heat. The overall reactions are as follows:

Anode:	$2\ H_2$	$\rightarrow$	$4\ H^+ + 4\ e^-$
Cathode:	$O_2 + 4\ H^+ + 4\ e^-$	$\rightarrow$	$2\ H_2O$
Combined:	$2\ H_2 + O_2$	$\rightarrow$	$2\ H_2O$

A schematic of a single PEMFC is given in Figure 1. Depending on the detailed operating conditions the product water can be in the liquid or gas phase. Above reaction occur inside the catalyst layers (CL's) and this means that the product water has to travel though the porous CL's and the porous transport

WIT Transactions on Engineering Sciences, Vol 70, © 2011 WIT Press
www.witpress.com, ISSN 1743-3533 (on-line)
doi:10.2495/MPF110251

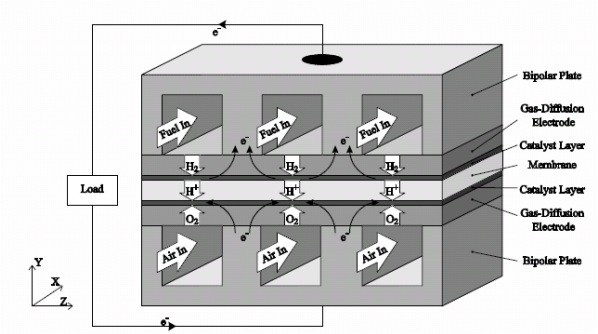

Figure 1: PEMFC schematic.

layers (PTLs) towards the flow channels where it can be picked up by the reactant.

The primary mechanism that drives the liquid water through the porous sublayers is capillary action, as was shown by Sinha and Wang [1], which is a diffusion-like mechanism that drives the water from regions of high concentrations to regions of low concentrations. The capillary pressure itself is a function of the material parameters of the porous material (contact angle, permeability, porosity) and of the liquid water volume fraction, also called "saturation". A frequently used equation to define the capillary pressure is the Leverett function, but recently there has been experimental effort to measure the capillary pressure as function of the saturation. Numerical models based on CFD typically use the Leverett function (described below) and may vary the coefficients in order to account for the pore-size distribution (PSD).

A common problem in these models has been the description of the liquid phase boundary condition at the interface between the porous gas diffusion layer (GDL) and the gas flow channel. A frequent approach was to specify a capillary pressure of zero at this interface, which corresponds to having a negligible amount of liquid phase at this interface. This was done by Berning and Djilali [2], among others. Alternatively, an arbitrary non-zero liquid saturation was prescribed by Natarajan and Nguyen [3] which ended up dominating the amount of liquid saturation inside the porous media. A more elaborate interfacial coverage model was proposed by Meng and Wang [4] in order to relate the liquid saturation at the interface to the cell potential and flow conditions in the channel. However, specifying any fixed value, either a value for the saturation or a capillary pressure, will not necessarily capture essential physics, as was pointed out by Gurau et al. [5]. This group in turn considered pending droplets, which are fed by one or more capillaries, and claim that the pressure downstream of the capillaries is equal to the pressure in the attached droplets which they feed. This means that equilibrium is assumed between the droplet and the pore that is feeding it. Such equilibrium must be questioned as it is an experimental observation that droplets continue to grow at a lower channel gas stream, which means that the capillary pressure of the pore feeding the droplet must always be larger than the capillary pressure of the sessile droplet. Weber and Newman [6]

assumed a zero liquid water flux if the gas phase pressure exceeds the liquid phase pressure while the capillary pressure is set to zero otherwise.

From a modelling perspective it is desirable to de-couple the transport phenomena inside the porous media from the channel, i.e. to prescribe a boundary condition where the GDL is not affected by the channel flow. The channel flow in turn will always be disturbed by the growing droplets, but these phenomena are very difficult to simulate in a model. Recently our group has suggested an approach of prescribing a boundary condition by applying a liquid phase pressure gradient across the interface at the last layer of the GDL [7]. This pressure gradient is derived from the Hagen-Poiseuille equation and is based on the experimental observation that liquid phase typically enters the channel through the same, "active" pores of the GDL [8]. It was found experimentally that the liquid water level inside the porous layers could be changed by perforating the GDL. In this work we want to investigate the effect of the boundary condition that our group has suggested on the predicted water content inside the porous media. A rendering of the liquid water transport is shown in Figure 2 [9].

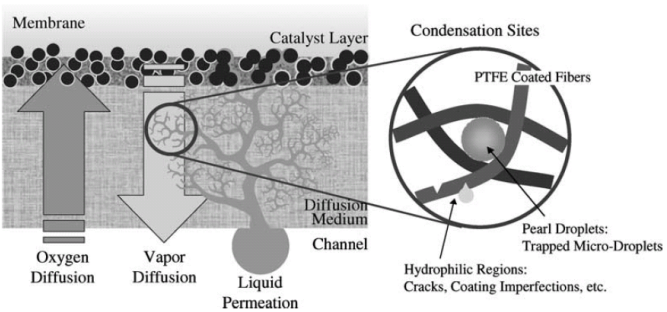

Figure 2: Rendering of the water transport model [9].

2 Model description

For the sake of brevity we do not list in detail all modelling equations employed in our comprehensive three-dimensional, non-isothermal CFD model. Instead we want to limit the list of equations to the description of liquid water flux through the porous media and across the GDL/channel interface.

As was previously shown, the three-dimensional momentum equations for the liquid phase in our multi-fluid model can be reduced to Darcy's law for the gas phase and liquid phase [7]:

$$\mathbf{u}_g = \frac{k_{rel,g} K}{\mu_g} \nabla p_g \tag{1}$$

$$\mathbf{u}_l = \frac{k_{rel,l} K}{\mu_l} \nabla p_l = \frac{k_{rel,l} K}{\mu_l} \nabla p_g - \frac{k_{rel,l} K}{\mu_l} \nabla p_{cap} \tag{2}$$

where the capillary pressure is defined as:

$$p_{cap} = \sigma \cos\theta \left(\frac{\varepsilon}{K}\right)^{0.5} J(S) \tag{3}$$

In above equations $\mathbf{u_g}$ and $\mathbf{u_l}$ are the three-dimensional velocity vectors, k_{rel} is the relative permeability of each phase, K is the dry permeability of the porous medium, μ is the dynamic viscosity and p is the pressure. Moreover, σ denotes the surface tension between the gas phase and the liquid phase (here 0.0625 *N/m*) and θ is the effective contact angle between the liquid phase and the porous medium. Here and in the following the subscripts "*g*" and "*l*" denote the gas phase and liquid phase, respectively. It is also important to realize that the terms including the permeability and the viscosity represent a flow resistance in Darcy's law. Thus the resistance for the liquid phase may be denoted:

$$R_{Darcy,l} = \frac{\mu_l}{k_{rel,l} K} \tag{4}$$

The relative permeability of the liquid phase depends on the volume fraction of the liquid phase inside the porous media, termed liquid saturation *s*, according to:

$$k_{rel,l} = s^n \tag{5}$$

where *s* is the liquid saturation and *n* is a prescribed exponent. In this work we apply a value of *n*=3.

The inverse of the property $(\varepsilon/K)^{0.5}$ is known as the characteristic pore-radius of the porous medium in question:

$$r_c^{-1} = \left(\frac{\varepsilon}{K}\right)^{0.5} \tag{6}$$

The Leverett *J*-function is typically of cubic nature, and our group has previously argued that it must be closely related to the integrated pore-size distribution (PSD), starting from the largest pores.

$$J(S) = 1.417S - 2.120S^2 + 1.263S^3 \tag{7}$$

A schematic of the liquid pressure as function of the saturation level for two different porous media is shown in Figure 3. For hydrophobic porous media the liquid pressure exceeds the gas phase pressure and the capillary pressure is negative.

Eqn. (3) also shows that different porous media have different capillary pressure functions. In a fuel cell there are porous layers with different material properties adjacent to each other. Because of the continuity of the pressure fields

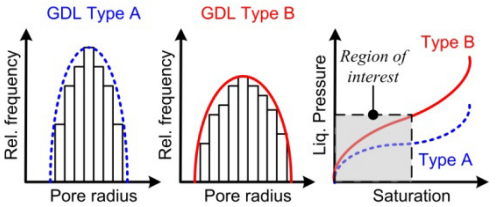

Figure 3: Expected liquid pressure curves for two types of porous media.

this leads to jump conditions for the liquid saturation across these interfaces. These jump conditions occur for example at the interface between the catalyst layer and the micro-porous layer as well as between the micro-porous layer and the GDL. Figure 4 shows schematically the capillary pressure curves for two different porous media and the arising jump in the liquid water saturation caused by the continuity in the capillary pressure across such an interface.

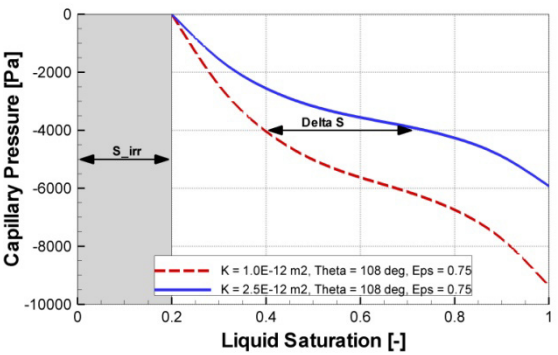

Figure 4: Capillary pressure versus saturation for two different material types.

While the above equations are sufficient to describe the capillary liquid water transport through the various porous layers in a fuel cell including the interface conditions, an important question still concerns the boundary condition for the liquid phase at the interface between the porous GDL/PTL and the gas flow channel.

In contrast to specifying fixed values for the capillary pressure or saturation at the GDL/channel interface our group has suggested to specify the liquid pressure gradient based on the Hagen-Poiseuille equation which relates the liquid phase velocity to the pressure gradient according to:

$$\mathbf{U}_l = -\frac{1}{8}\frac{r_c^2}{\mu_l}\nabla p_l = -\frac{1}{8}\left(\frac{K}{\varepsilon}\right)\frac{1}{\mu_l}\nabla p_l \tag{8}$$

In this equation $\mathbf{U_l}$ denotes the intrinsic velocity which is related to the superficial velocity in the through-plane direction according to:

$$V_l A_{pores} = v_l A_y \tag{9}$$

where V_l is now the intrinsic velocity component in the y-direction of the liquid phase described by the Hagen-Poiseuille equation and v_l is the superficial velocity component that corresponds to the velocity field that CFX-4 calculates.

Combining the last two equations yields:

$$v_l = \frac{A_{pores}}{A_y} V_l = \frac{n_{pores} \times \pi \times r_c^2}{A_y} V_l = -n''_{pores} \frac{\pi}{8} \left(\frac{K}{\varepsilon} \right)^2 \frac{1}{\mu_l} \frac{\partial p_l}{\partial y} \tag{10}$$

In above equation the number of pores in the cell area in y-direction A_y is related to the number of pores per unit area according to:

$$n_{pores} = n''_{pores} A_y \tag{11}$$

where n_{pores} is the number of "active" pores in the control volume under consideration, and a control volume is a volume element in the numerical grid of the CFD model. The area of the control volume in the y-direction is denoted A_y, and we are only considering those volume elements located inside the GDL adjacent to the flow channels.

Eqn. (10) denotes again the liquid flow velocity as function of a resistance and the driving pressure gradient, and the resistance is in this case:

$$R_{H.-P.} = \frac{1}{n''_{pores}} \frac{8}{\pi} \left(\frac{\varepsilon}{K} \right)^2 \mu_l \tag{12}$$

Hence we have described two resistances, the Darcian resistance which depends on the liquid saturation and the Hagen-Poiseuille resistance which depends on the number of active sites per unit area. This resistance is only invoked at the GDL/channel interface in order to capture the experimental observation that the liquid phase enters the channel through a number of open, "active" pores that are the same over a wide range of operating conditions. A comparison of the order of magnitude of the Darcian resistance to the Hagen-Poiseuille resistance is shown in Figure 5. The porosity in this case is $\varepsilon = 75\%$ and the dry permeability of $K = 1$ Darcy $= 10^{-12}\ m^2$. According to Eqn. (5) the Darcy resistance also depends on the exponent in the relative permeability, while the overall resistance in the Hagen-Poiseuille expression depends on the number of active sites for unit area which is in the order of $10^6\ m^{-2}$.

In our code the Hagen-Poiseuille resistance is only implemented for the last layer of fibres between the GDL and the flow channel. In the interior we consider Darcian resistance only. When we consider the flow exiting through the last pore we need to estimate the length of these pores on order to obtain the expected pressure drop. The carbon fibres of the GDL typically have a diameter of 7–10 μm, and so we estimated the pore length for the Hagen-Poiseuille flow to

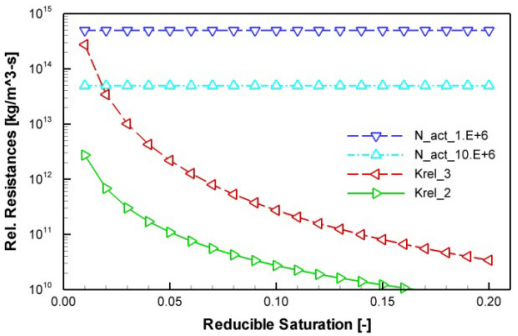

Figure 5: Comparison between the Hagen-Poiseuille and Darcian resistance.

be $l_p = 4\ \mu m$. In a pore network model this properties typically call the "throat length".

In our CFD code we need to combine both resistances due to the fact that the cell height of the control volumes in our numerical grid at the GDL/channel interface is larger than the outlet pore height, which we may leave adjustable. Hence we need to account for a Darcian resistance and a resistance at the outlet pores in the same control volume, where the superficial velocity as calculated by the CFD code is the same in both resistance regions, but the pressure drops are additive and combine to yield the pressure gradient as calculated by the CFD code.

Denoting the height of the control volume dy_c yields for the Darcian part:

$$v_l = \frac{1}{R_{Darcy,y}} \frac{\Delta p_{l,Darcy,y}}{\left(dy_c - l_p\right)} \tag{13}$$

The height of the control volume depends on the grid size and typically ranges around 20 – 30 μm. The Hagen-Poiseuille equation applies to the pore height l_p and yields:

$$v_l = \frac{1}{R_{H-P,y}} \frac{\Delta p_{l,H-P,y}}{l_p} \tag{14}$$

The pressure drops are additive to yield the pressure drop over the entire control volume according to:

$$\Delta p_{l,y} = \Delta p_{l,Darcy,y} + \Delta p_{l,H-P,y} \tag{15}$$

Finally it holds for the superficial velocity:

$$v_l = \frac{1}{R_{\text{int},y}} \frac{\Delta p_{l,y}}{dy_c} \tag{16}$$

where $R_{int,y}$ is now the combined resistance at the GDL/channel interface as it is implemented in our CFD model. This can be expressed as function of the partial resistances due to Darcy and Hagen-Poiseuille:

$$R_{\text{int},y} = \ldots = \left(1 - l_p / dy_c\right) R_{Darcy} + \left(l_p / dy_c\right) R_{H-P} \tag{17}$$

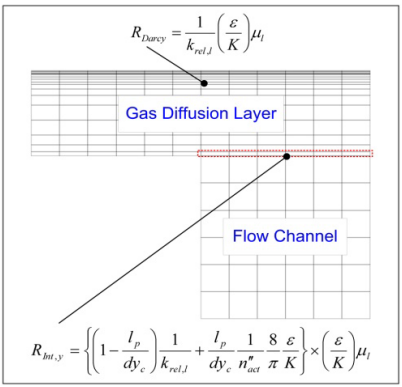

Figure 6: Local resistances inside the porous layers and numerical grid.

Figure 6 shows schematically the numerical grid of the cathode porous layers and gas flow channel and the resistance terms implemented. As described above the resistance due to the Hagen-Poiseuille equation is only implemented at the control volume of the GDL that are adjacent to the gas flow channel.

3 Model results

Clearly the complete model is much more complex than described above as it also contains multi-species flow at the cathode and anode side, heat transfer including phase change, electrochemical reactions and water transport through the electrolyte membrane. However, in this study we want to focus on the description of the liquid phase transport through the porous media by capillary action.

The model was applied to study the behaviour of a PEMFC operating at a current density of 0.4 A/cm^2. The cell temperature is 353 K and the operating pressure is 1.5 atm (total) at the outlet. Both the air at the cathode and the hydrogen at the anode are humidified to 75% RH at the inlet, and the stoichiometric flow ratio is 3 at both anode and cathode side. In a previous study we have found that the specific surface area of the electrolyte phase in the CLs is very important for the overall water balance [10]. In this study we have employed a value of 5.0×10^4 m^2/m^3, which is comparatively low and ensures that the cathode side becomes flooded, which is essential for this study. Because the primary focus of the current study is the role of the boundary condition for the

liquid phase at the GDL/channel interface, the main parameter that was varied in this study is the number of active sites per unit area n_{act}".

The important material properties applied inside the porous media are summarized in Table 1. The fact that all porous regions were assigned different material properties leads to a jump condition for the liquid saturation according to Figure 4. The effective contact angle that is used to calculate the capillary pressure was $\theta = 120^{o}$ for all porous regions. Of note is that this value only applies to the hydrophobic pores while the hydrophilic pore fraction is included in the irreducible saturation.

Table 1: Material parameters of the different porous regions.

Porous Region	Porosity [-]	In-plane permeability [m^2]	Through-plane permeability [m^2]	Irreducible saturation [-]
CL	75%	1.E-12	1.E-12	0.3
MPL	75%	1.E-12	1.E-12	0.2
GDL	75%	20 E-12	10 E-12	0.2

For the sake of brevity we can only show a few results. Figures 7–9 show the predicted liquid saturation inside the porous media at the cathode side at mid-channel (the total channel length investigated is 25 *mm*). The results have been mirrored in the postprocessor for better visualization. The difference in these cases is only the variation in the number of active pores per unit area n_{act}". Figure 7 is for the case of a non-modified boundary condition, where the pore length l_{pore} has been set to zero in our code which means that the standard Darcy resistance has not been modified. Figures 8 and 9 are for the case of n_{act}" = 10×10^6 and n_{act}" = 1×10^6, respectively. The visualization results as published by Zhang et al. [8] show that these are realistic values. The results indicate no discernible effect between the cases of having no additional resistance and having n_{act}" = 10×10^6, *i.e.* 10 active sites per mm^2. For an active site density of 1×10^6 there is a noticeable increase in liquid saturation, *i.e.* the boundary condition has an impact on the predicted modelling results. Of note is that the number of active sites per unit area was observed to be in exactly this region, i.e. around 1–10 mm^{-2} [8].

Figures 10–12 show the predicted liquid saturation inside the porous GDL in a cut close to the channel interface. Hence the liquid volume fraction under the channel area and under the land area of fuel cell can be seen. Again the main differences can be observed between the case of n_{act}" = 10×10^6 and n_{act}" = 1×10^6, hence in the physically realistic regime. Reducing the number of active sites per unit area leads to an increase in flow resistance for the liquid phase in the through-plane direction. Hence the water spreads out more in the in-plane direction. In any case we observe that the boundary condition as we have implemented it does have an impact on the modelling results. Gerteisen et al. [11] have found that drilling holes into the GDL to release the liquid water can stabilize the cell performance.

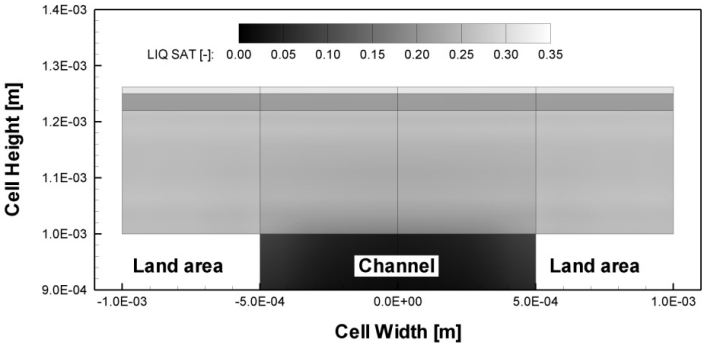

Figure 7: Predicted liquid saturation inside the cathode side porous media at mid-channel for the case of the "standard" boundary condition (l_{pore}=0 μm).

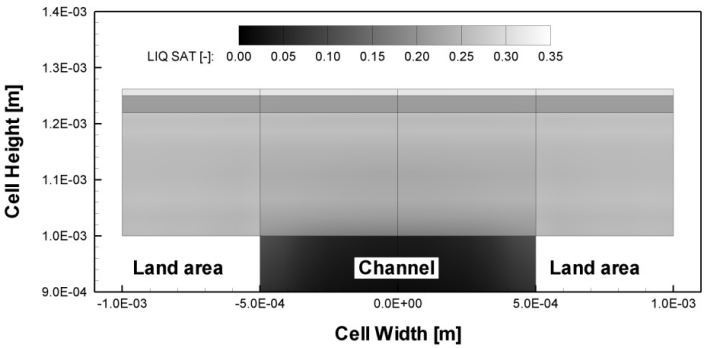

Figure 8: Predicted liquid saturation inside the cathode side porous media at mid-channel for the case of n_{act}"= 10 mm^{-2}.

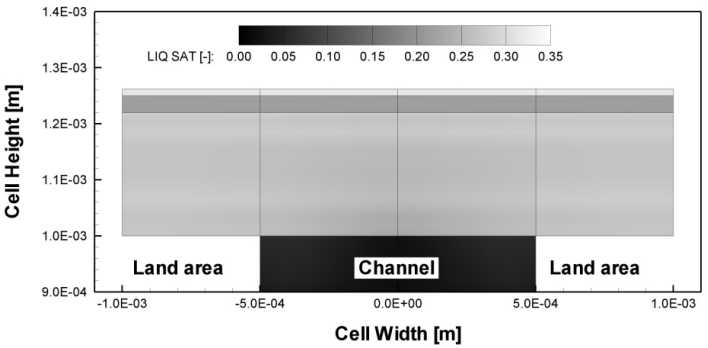

Figure 9: Predicted liquid saturation inside the cathode side porous media at mid-channel for the case of n_{act}"= 1 mm^{-2}.

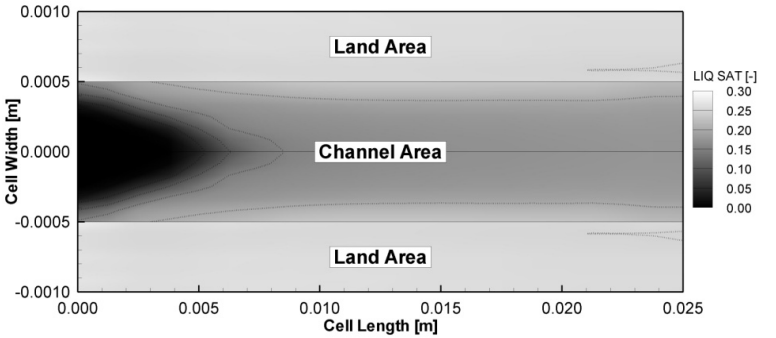

Figure 10: Predicted liquid saturation inside the cathode GDL close to the channel interface for the case of the "standard" boundary condition (l_{pore}=0 μm).

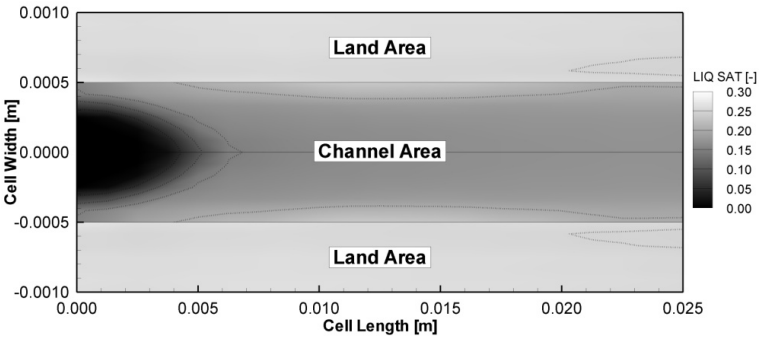

Figure 11: Predicted liquid saturation inside the cathode GDL close to the channel interface for the case of n_{act}"= 10 mm^{-2}.

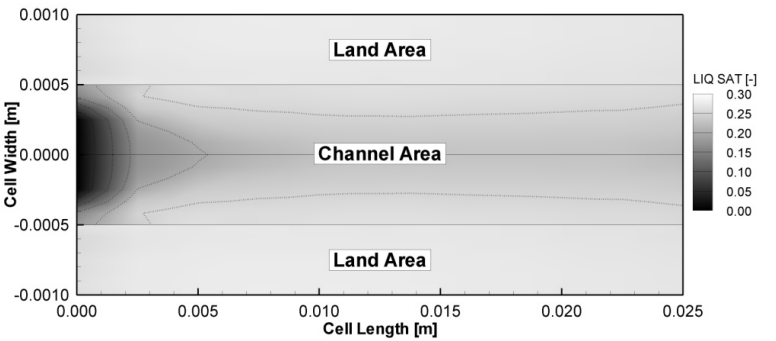

Figure 12: Predicted liquid saturation inside the cathode GDL close to the channel interface for the case of n_{act}"= 1 mm^{-2}.

4 Conclusions

We have proposed a novel boundary condition for the liquid phase at the GDL/channel interface of a PEM fuel cell. This boundary condition is based on the experimental observation that there are only a few pores per mm^2 that release the liquid water, and this means that the frequently use Darcy approach may not be applicable for this flow regime. Instead, we have utilized the Hagen-Poiseuille equation to describe the pressure drop across the outlet pores. This was implemented as an additional resistance for the liquid phase at the channel/GDL boundary. First simulations indicate that this boundary condition has a significant impact on the predicted liquid saturation inside the porous media. This is in good accord with experimental observations. More work is needed to fully understand and quantitatively verify this effect.

References

[1] Sinha, P. K. & Wang, C.-Y.: Pore-network modeling of liquid water transport in gas diffusion layer of a polymer electrolyte fuel cell, Electrochimica Acta, 52 (2007) 7936-7945.
[2] Berning, T. & Djilali, N.: A 3D, multiphase, multicomponent model of the cathode and anode of a PEM fuel cell, J. Electrochem. Soc. 150 (2003) A1589-A1598.
[3] Natarajan, D. & Nguyen, T. V.: Three-dimensional effects of liquid water flooding in the cathode of a PEM fuel cell, J. Power Sources 115 (2003) 66.
[4] Meng, H. & Wang, C.-Y.: Model of two-phase flow and flooding dynamics in polymer electrolyte fuel cells, J. Electrochem. Soc. 152 (2005) A1733-A1741.
[5] Gurau, V., Zawodzinski, T. A. & Mann J. A.: Two-phase transport in PEM fuel cell cathodes, J. Fuel Cell Science and Technology 5 (2008) 021009.
[6] Weber, A. Z. & Newman, J.: Effects of microporous layers in polymer electrolyte fuel cells, J. Electrochem. Soc. 152 (2005) A677-A688.
[7] Berning, T., Odgaard, M. & Kær, S.: A computational analysis of multi-phase flow through the porous media of a PEMFC cathode using the multi-fluid approach, J. Electrochem. Soc. 156 (2009) B1301.
[8] Zhang, F. Y., Yang, X. G. & Wang, C.-Y.: Liquid water removal from a polymer electrolyte fuel cell, J. Electrochem. Soc. 153 (2006) A225-A232.
[9] Nam, J. H. & Kaviany, M.: Effective diffusivity and water-saturation distribution in single- and two-layer PEMFC diffusion medium, Int. J. Heat Mass Transfer 46 (2003) 4595-4611.
[10] Berning, T., Odgaard, M. & Kær, S.: Water Balance Simulations of a PEM Fuel Cell Using a Two-Fluid Model, ECS Trans. 33 (2010) 1503-1513.
[11] Gerteisen, D., Heilmann, T. & Ziegler, C.: Enhancing liquid water transport by laser perforation of a GDL in a PEM fuel cell, J. Power Sources 177 (2008) 348.